Experimental Verification of the Van Vleck Nature of Long-Range Ferromagnetic Order in the Vanadium-Doped Three-Dimensional Topological Insulator Sb_2Te_3

Mingda Li,[1,2,3,*,†] Cui-Zu Chang,[2,*,‡] Lijun Wu,[3] Jing Tao,[3] Weiwei Zhao,[6] Moses H. W. Chan,[6] Jagadeesh S. Moodera,[2,5] Ju Li,[1,4] and Yimei Zhu[3,*,§]

[1]*Department of Nuclear Science and Engineering, Massachusetts Institute of Technology, Cambridge, Massachusetts 02139, USA*
[2]*Francis Bitter Magnet Lab, Massachusetts Institute of Technology, Cambridge, Massachusetts 02139, USA*
[3]*Condensed Matter Physics and Materials Science Department, Brookhaven National Laboratory, Upton, New York 11973, USA*
[4]*Department of Material Science and Engineering, Massachusetts Institute of Technology, Cambridge, Massachusetts 02139, USA*
[5]*Department of Physics, Massachusetts Institute of Technology, Cambridge, Massachusetts 02139, USA*
[6]*The Center for Nanoscale Science and Department of Physics, The Pennsylvania State University, University Park, Pennsylvania 16802-6300, USA*

(Received 18 December 2014; revised manuscript received 13 February 2015; published 9 April 2015)

We demonstrate by high resolution low temperature electron energy loss spectroscopy (EELS) measurements that the long range ferromagnetic (FM) order in the vanadium- (V-)doped topological insulator Sb_2Te_3 has the nature of van Vleck–type ferromagnetism. The positions and the relative amplitudes of two core-level peaks (L_3 and L_2) of the V EELS spectrum show unambiguous change when the sample is cooled from room temperature to $T = 10$ K. Magnetotransport and comparison of the measured and simulated EELS spectra confirm that these changes originate from the onset of FM order. Crystal field analysis indicates that in V-doped Sb_2Te_3, partially filled core states contribute to the FM order. Since van Vleck magnetism is a result of summing over all states, this magnetization of core level verifies the van Vleck–type ferromagnetism in a direct manner.

DOI: 10.1103/PhysRevLett.114.146802 PACS numbers: 73.20.-r, 75.50.Pp, 79.20.Uv

The breaking of time-reversal symmetry and the opening of a surface band gap of a topological insulator (TI) is an essential step towards observing other quantum states [1–3]. When the TI's chiral Dirac surface state is gapped, a number of promising novel phenomena could be realized, including the quantum anomalous Hall effect (QAHE) [3–10], where spontaneous magnetization and spin-orbit coupling lead to a topologically nontrivial electronic structure, and the topological magneto-electric effect results through coupling between electric field and spin texture, which can potentially lead to low-power electrically controlled spintronic devices [11–15]. There are two generic approaches to break the time-reversal symmetry: by the magnetic proximity effect or by conventional transition metal (TM) doping [1,16–18]. Doping TM impurities (i.e., V, Cr, Mn) into TI can induce a perpendicular ferromagnetic (FM) anisotropy, providing a straightforward method to open up the band gap of the TI's chiral surface state and tune the corresponding transport properties [7,8,19–23]. In diluted magnetic semiconductors doped with TM atoms, the induced FM order in general originates from itinerant charge carriers [24,25], i.e., the Ruderman-Kittel-Kasuya-Yosida (RKKY)-mediated FM order. However, in magnetically doped TI, the itinerant carriers may destroy the QAHE by providing additional conduction channels [26], resulting in a leakage current [12,27], which severely hinders the magnetic TI for device applications. Therefore, a carrier-free yet long range mechanism to induce FM order in magnetically doped TI's is highly desirable for progress towards device applications.

On the other hand, in a magnetically doped TI, the first-principles calculations predicted that the insulating magnetic ground state can indeed be obtained by a proper choice of TM dopants, through van Vleck–type ferromagnetism in the absence of itinerant carriers [5]. Recently, Chang *et al.* [7,8] has reported experimental observation of QAHE in magnetic TI Cr- and V-doped $(Bi, Sb)_2Te_3$, where the insulating FM order [23] excludes the RKKY-type interaction and indicates the FM mechanism to be of van Vleck–type as first-principles calculations predicted. In such a system, the inverted band structure in TI leads to the large matrix element of the valence band [5,23,26], dramatically increasing the contribution to spin susceptibility. Since the van Vleck–type susceptibility is directly related with 2nd order energy perturbation as 2nd order derivate $\chi = -d^2E_0^{(2)}/dH^2$ [28], one could understand the van Vleck–type mechanism qualitatively from 2nd order perturbation theory, as shown in Eq. (1),

$$E_0^{(2)} = \sum_n \frac{|\langle 0|\mu_B(\vec{L} + g\vec{S}) \cdot H|n\rangle|^2}{E_0 - E_n}. \quad (1)$$

Here, $\sum$ denotes the summation over all electronic states of Vanadium. Noticing that written in this way, the meaning of van Vleck magnetism is not quite the same as [5], where

spin susceptibility of electrons in TI is calculated and V ions are considered as dopants. Here, we focus on the van Vleck magnetism of V itself. In this sense, Eq. (1) is a summation of all Vanadium states hence has both intra-atomic and inter-atomic origins [29], while only the inter-atomic part deals with the interactions with TI electrons as in [5]. Our results, on the other hand, show that the intra-atomic contribution to the van Vleck magnetism. Moreover, based on [5], the finite density of state near the Fermi level excludes the possibility to have QAHE in V-doped TI, while the very recent experimental observation of QAHE in V-doped TI [7] supports a picture of van Vleck magnetism from other origin. The core-level related intra-atomic van Vleck magnetism is a reasonable origin to support the QAHE in V-doped TI.

In this *Letter*, we report the magnetization of partially filled vanadium (V) $2p_{3/2}$ and $2p_{1/2}$ (L_3 and L_2) core states, using low-temperature high-resolution electron energy loss spectroscopy (EELS). The condition for partial filling of core states is achieved when a high-energy incidence of electrons on a sample in a transmission electron microscope (TEM) excites a core electron to unoccupied states leaving a core hole behind, giving to the energy-loss spectrum. Analyzing the fine structure of the energy-loss spectrum provides not only the information on the unoccupied local density of states, but also the angular momentum, spin, and chemical nature of the element. We find that by comparing with the room temperature (RT) spectrum, the Te $M_{4,5}$ edge at $T = 10$ K shows no shift, while the V L_3 and L_2 peaks show a redshift as large as 0.6 eV. In addition, there is a clear drop of the L_3/L_2 peak intensity ratio. EELS simulation with FEFF 9 [30–32] shows that such shift is a signature of onset of FM order, which is independently verified through magnetotransport results, where the anomalous Hall effect below the Curie temperature $T_c \sim 70$ K is revealed.

High-quality V-doped Sb_2Te_3 films are grown by molecular beam epitaxy (MBE) under a base vacuum $\sim 5 \times 10^{-10}$ Torr, where thin film Sb_2Te_3 (111) was grown on top of etched Si (111) substrates with V dopants coevaporated from an electron beam source during TI growth. Ultrathin cross sectional TI film samples are fabricated through focused ion beam and postprocessing for high-resolution TEM studies. The EELS measurements were carried out using the doubled aberration corrected JEM-ARM200CF TEM, equipped with a cold field-emission gun and the state-of-the-art duel energy-loss spectrometer (Quantum GIF). V-doped Sb_2Te_3 samples still maintain a very good layered structure [Fig. 1(a)], due to the likely case that V dopants tend to substitute Sb sites instead of creating interstitials [7]. The selected area electron diffraction pattern [Fig. 1(b)] along the [0001] zone-axis direction also verifies the negligible influence of V dopants to the crystal structure, in that the V-doped

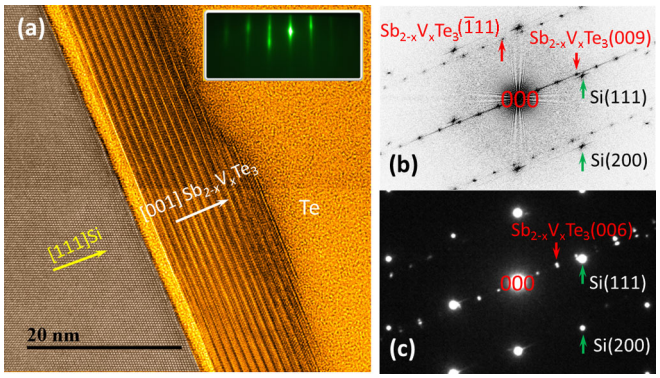

FIG. 1 (color online). (a) High-resolution image of the V-doped Sb_2Te_3 sample S3 grown on an etched Si substrate (bottom-left, brown region) viewed along the $[\bar{1}\,\bar{1}\,0]$ direction of $Sb_{2-x}V_xTe_3$. Another capping layer (top-right, yellow region) is mainly composed of amorphous Te protection layers. The upper right inset is a reflection of the high-energy electron diffraction (RHEED) image showing the ultrahigh crystalline quality of the MBE-grown film. (b) Diffractogram from (a). One set of spots as indicated by green arrows can be indexed as a $(0\bar{1}1)$ pattern of Si, while the other set of spots indicated by red arrows can be indexed as a $(\bar{1}\,\bar{1}\,0)$ pattern of a rhombohedral lattice with $a = 0.42$ and $c = 3.03$ nm, which is basically the same as the Sb_2Te_3 lattice, indicating negligible influence of V dopants to the lattice. The [001] Sb_2Te_3 is slightly misaligned (~3°) with [111] Si. (c) Select-area electron diffraction pattern from the area containing both the film and substrate.

Sb_2Te_3 has an almost identical lattice constant compared with that of pure Sb_2Te_3.

Figure 2 shows the main result of this Letter comparing with the EELS spectra in the high-loss region at RT and low temperature $T = 10$ K. A simultaneous collection of both low-loss and high-loss spectra allows for a high-accuracy positioning of the zero-loss peak, thus accurate energy scale calibration. We see clearly that the $M_{4,5}$ edge of the Te element does not shift with temperature, while there are obvious peak position shifts (>0.5 eV) for both V L_3 and L_2 peaks, accompanied with a decrease in the L_3/L_2 ratio.

In order to verify the observed peak shift, we measured three samples of $Sb_{2-x}V_xTe_3$ with different V concentrations and thicknesses, namely, sample S1: 20 quintuple layer (QL) with $x = 0.08$, S2: 20 QL with $x = 0.16$, and S3: 12 QL with $x = 0.08$. The corresponding mean V-V distances in all the samples are thus ≥10 nm. Since EELS is a spatially highly localized probe and there might be small nonuniformity of dopants, we collected 8 spectra at both 10 K and RT for each sample to reduce the measurement uncertainty. Furthermore, we use two different algorithms to extract the peak positions. The averaged V L_3 and L_2 peak positions and L_3/L_2 ratios for all the three samples are plotted in Figs. 3(b)–(d).

All three samples show the same trend that the L_3 and L_2 peak positions at $T = 10$ K [blue and green dots in

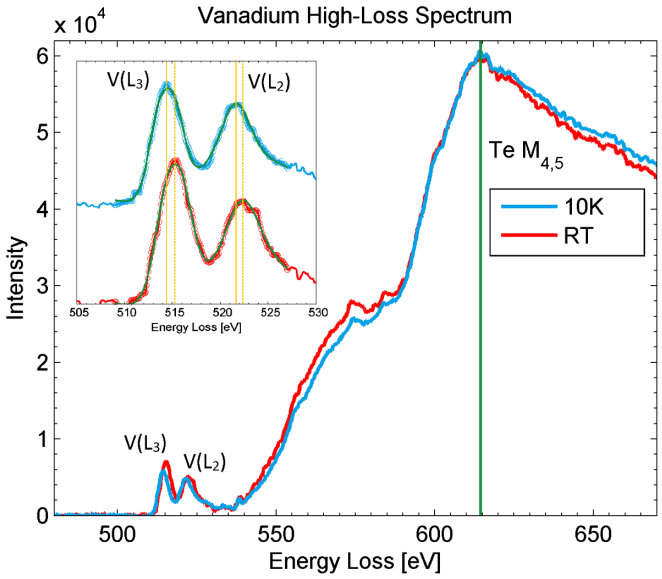

FIG. 2 (color online). EELS spectra of V L and Te $M_{4,5}$ edges at RT (red curve; lower curve in inset) and 10 K (blue curve; upper curve in inset) for sample S2, normalized with Te $M_{4,5}$ edge intensity. The energy position of Te $M_{4,5}$ edge is invariant of temperature (green vertical line ~615 eV), while there is a clear redshift of vanadium's L_3 and L_2 positions (yellow vertical lines in inset) and a drop of L_3/L_2 ratio. The energy scale has been accurately calibrated by simultaneously acquiring and aligning of the zero-loss peak.

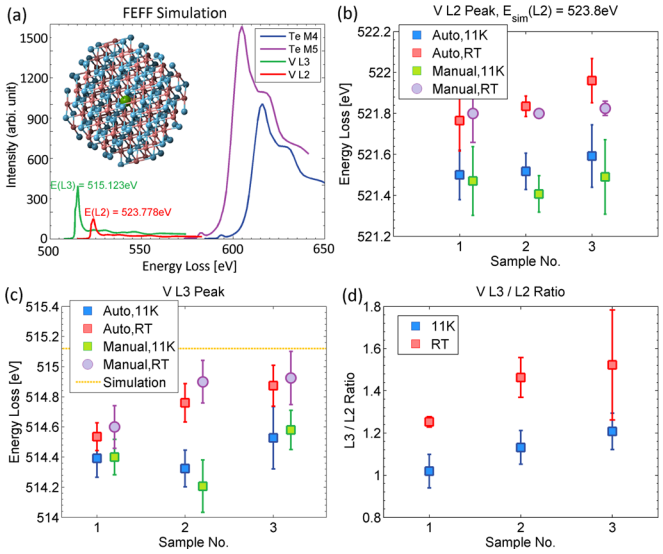

FIG. 3 (color online). (a) FEFF simulation of the high-loss EELS spectrum of V-doped Sb_2Te_3, using a nanosphere (inset) with a scattering center in the middle. (b)–(d) Experimental EELS peak positions and shifts. (b) The V-L_2 peak positions, showing a similar trend of redshift for all three samples. The two algorithms show consistent results. (c) The V-L_3 peak positions, where sample S2 with the highest V concentration shows the highest redshift. A horizontal yellow line marks the energy position from nonmagnetic simulation, which is slightly higher than the RT magnitudes. (d) The V's L_3/L_2 peak intensity ratio change. At $T = 10$ K, the ratio drops, which is also consistent with the simulation, where for a nonmagnetic system the ratio is even higher.

Figs. 3(b) and 3(c)] undergo a redshift compared with RT (red and purple dots). For the L_2 peaks, all three samples shift similar amounts ~0.4 eV, while for the L_3 peak positions, the shift ranges from 0.3 (samples S1 and S3) to 0.7 eV (sample S2). This indicates that at low temperature, a certain mechanism, which does not change Te states, alters the L_3 and L_2 core states of V. The higher concentration of V tends to yield a stronger energy reduction of the L_3 peaks. In addition, the L_3/L_2 ratio drops from ~1.4 to 1.1 (samples S2 and S3), indicating a possible change of electronic structure or even a phase transition [33].

To understand the possible origin of the peak position shift and peak intensity ratio drop, we simulate the EELS spectrum with a nonmagnetic V-doped TI nanosphere using FEFF 9 [Fig. 3(a), inset]. We take 1.0 nm for the full multiple scattering cutoff radius and 0.5 nm for the self-consistent-field cutoff radius to ensure convergence, with Hedin-Lundqvist self-energy and random phase approximation with core-hole correction. The resulting nonmagnetic peak positions give $E(L_3) = 515.1$ and $E(L_2) = 523.8$ eV, which are both higher than the magnitude at RT. The higher V energy for a nonmagnetic system is quite reasonable, since even at RT, there is already partial magnetization due to the field in the sample areas from the objective lens of the microscope. In other words, the redshift of V L_3 and L_2 peaks is consistent with a picture that a nonmagnetic system has even higher energy.

As shown in Fig. 3, the different amount of redshift for L_3 and L_2 edges is consistent with a temperature-independent Te $M_{4,5}$ position at ~615 eV. Sample S2 with the highest V concentration ($x = 0.16$) shows the highest redshift, indicating that such a redshift has an origin related to strong V-V interaction. Moreover, since L_3 and L_2 edges have similar order of peak positions (around 515 and 521 eV), but different l-s spin coupling configuration, the different redshift amount between the L_3 and L_2 peaks further indicates that a spin-related process may play an important role in the V-V interaction.

Thus, the consistently observed trend at RT and $T = 10$ K of the energy redshift of V's L_3 and L_2 edge and the decrease of L_3/L_2 ratio from nonmagnetic simulations unambiguously indicates a change of electronic structure, while the very different redshift behavior between the L_3

TABLE I. Character table of irreducible representation $\Gamma^{(2)}_{\text{full}}$ for the full rotational group. When the crystal field is present, this becomes a reducible representation and the degeneracy is lifted.

χ	E	$2C_3$	$3C'_2$	I	$2S_6$	$3\sigma_d$
$\Gamma^{(2)}_{\text{full}}$	5	−1	+1	5	−1	+1

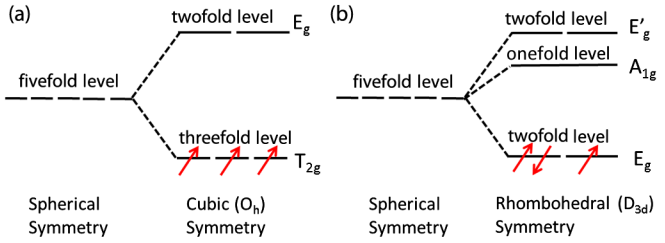

FIG. 4 (color online). (a) Crystal field splitting in the cubic crystal field. T_{2g} levels allow the spin alignment from all three $3d$ electrons of V (red arrows), leading to a possible FM order. (b) Crystal field splitting under rhombohedral D_{3d} crystal field. Since the energy only splits into a twofold level and only 1 electron has unpaired spin, it is too weak to form a FM order.

and L_2 peak together with a concentration dependence further indicates a magnetic origin from these core levels. Actually, this core-level magnetism for V dopants could also be understood through crystal field theory. For an $l = 2$ transition metal ion dopant (such as V), the character table of irreducible representation for the full rotational group is shown in Table I. The conjugacy classes are taken as the symmetry elements contained in TI's D_{3d} group. Under TI's rhombohedral D_{3d} crystal field, this irreducible representation $\Gamma^{(2)}_{\text{full}}$ becomes reducible, resulting in the lift of degeneracy and crystal field splitting.

From Table I and character table of D_{3d} group [34], we calculate the decomposition of the representation $\Gamma^{(2)}_{\text{full}}$ in D_{3d} group as

$$\Gamma^{(2)}_{\text{full}} = A_{1g} \oplus 2E_g; \tag{2}$$

i.e., instead of splitting to a twofold E_g and a threefold T_{2g} level which is the case of the octahedral crystal field, an $l = 2$ transition metal ion would split from a fivefold level to two twofold levels (E_g and E'_g) and one nondegenerate level A_{1g} (Fig. 4) under TI's rhombohedral crystal field.

Since V has electron configuration $[\text{Ar}]3\text{d}^3 4\text{s}^2$, this crystal field effect tends not to be important to explain why V's sole $3d$ electron state may not be sufficient to form FM order in TI. Unlike the cubic crystal field where a threefold T_{2g} state allows a parallel spin configuration [Fig. 4(a)], the twofold E_g level and Pauli's exclusion principle only lead to a single unpaired electron under the rhombohedral crystal field. This becomes too weak to form a long range FM order by solely $3d$ valence states [Fig. 4(b)]. Therefore, the FM order in V-doped TI may be mediated from other V states, such as core states. This is fully consistent with our EELS results for L_3 and L_2 core states at $T = 10$ K.

In order to further demonstrate that the V-doped Sb_2Te_3 system is indeed FM at $T = 10$ K, we perform magnetotransport measurement for both longitudinal and transverse directions. Temperature-dependent longitudinal dc resistivity at zero magnetic field [Fig. 5(a)] shows a resistivity hump at about 70 K, indicating the onset of FM order since the spin-disorder scattering is reduced [35]. Figure 5(b) shows a typical weak antilocalization behavior and butterfly shape above and below 70 K, indicating a non-FM–FM transition. This transition is further corroborated by Fig. 5(c), showing the hysteresis loop of the Hall resistance R_{yx}. The loop is closed above 70 K, which is consistent with the R_{xx} result. Hence, we conclude that the Curie temperature T_c is ~70 K, far above the EELS measurement temperature of $T = 10$ K. This independently verifies the FM order of our V-doped Sb_2Te_3 sample.

In conclusion, we have demonstrated the van Vleck nature of the FM order in V-doped TI Sb_2Te_3 using low-temperature high resolution EELS. An energy redshift is observed in V's L_3 and L_2 core states, which could be understood as a signature due to the onset of FM order, while the FM order itself is shown independently through magnetotransport measurement. The V-dopants' core-level contribution to the ferromagnetism in TI is thus in sharp contrast to the RKKY-type ferromagnetism, where only itinerant electrons contribute to the magnetic susceptibility regardless of the core level states, but consistent with the picture of van Vleck–type ferromagnetism, where the

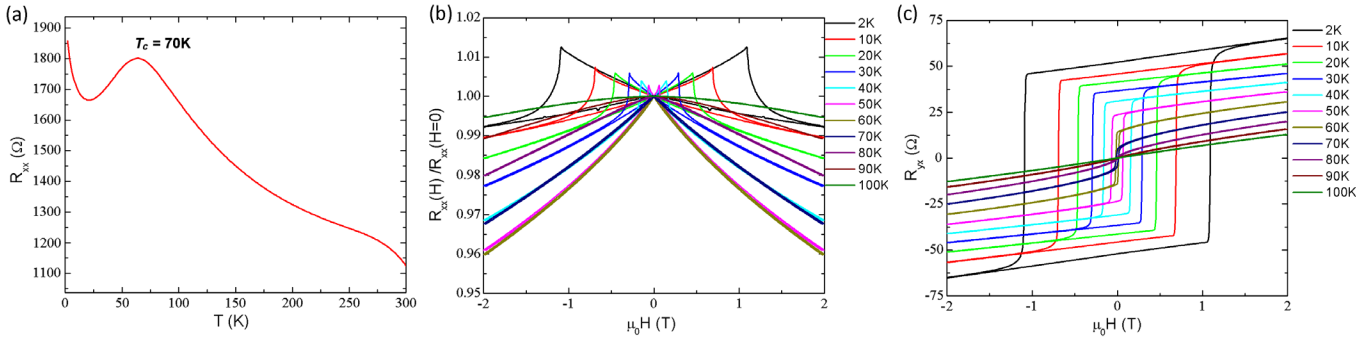

FIG. 5 (color online). (a) Longitudinal resistance R_{xx} as a function of temperature at zero field. (b) Normalized magnetic-field dependent longitudinal resistance R_{xx} at various temperature. Above 70 K, it shows weak antilocalization behavior, while below 70 K, the butterfly shape indicates the onset of FM order. (c) Magnetic-field dependent Hall resistance R_{xy}. The opening up of a hysteresis loop below 70 K is quite consistent with (a) and (b), indicating an onset of FM order.

susceptibility is a summation of contributions from all possible intermediate states. In this sense, although we could not exclude the contribution of RKKY interaction to the FM order from the band electrons, van Vleck mechanism, resulting from core levels and playing a significant role in FM order, is observed unambiguously. Such a core-level contribution could also be understood from a crystal-field perspective, where three $3d$ electrons under a rhombohedral crystal field could neither lead to FM order nor screen the contribution from the cores.

The work at the Brookhaven National Laboratory was supported by the U.S. Department of Energy, Office of Basic Energy Sciences under Contract No. DE-AC02-98CH10886. J. S. M. and C. Z. C would like to thank support from the STC Center for Integrated Quantum Materials under NSF Grant No. DMR-1231319, NSF DMR Grants No. 1207469 and ONR Grant No. N00014-13-1-0301. Work at Penn State was supported by NSF MRSEC program under Awards No. DMR-0820404 and No. DMR-1420620.

*To whom all correspondence should be addressed.
†mingda@mit.edu
‡czchang@mit.edu
§zhu@bnl.gov

[1] X. L. Qi and S. C. Zhang, Rev. Mod. Phys. **83**, 1057 (2011).
[2] M. Z. Hasan and C. L. Kane, Rev. Mod. Phys. **82**, 3045 (2010).
[3] C.-Z. Chang, P. Wei, and J. S. Moodera, MRS Bull. **39**, 867 (2014).
[4] X. L. Qi, T. L. Hughes, and S. C. Zhang, Phys. Rev. B **78**, 195424 (2008).
[5] R. Yu, W. Zhang, H. J. Zhang, S. C. Zhang, X. Dai, and Z. Fang, Science **329**, 61 (2010).
[6] C.-X. Liu, X.-L. Qi, X. Dai, Z. Fang, and S.-C. Zhang, Phys. Rev. Lett. **101**, 146802 (2008).
[7] C. Z. Chang *et al.*, Nat. Mater. **25**, 1065 (2015).
[8] C. Z. Chang *et al.*, Science **340**, 167 (2013).
[9] X. F. Kou *et al.*, Phys. Rev. Lett. **113**, 137201 (2014).
[10] J. G. Checkelsky, R. Yoshimi, A. Tsukazaki, K. S. Takahashi, Y. Kozuka, J. Falson, M. Kawasaki, and Y. Tokura, Nat. Phys. **10**, 731 (2014).
[11] A. M. Essin, J. E. Moore, and D. Vanderbilt, Phys. Rev. Lett. **102**, 146805 (2009).
[12] L. A. Wray, Nat. Phys. **8**, 705 (2012).
[13] R. D. Li, J. Wang, X. L. Qi, and S. C. Zhang, Nat. Phys. **6**, 284 (2010).
[14] F. X. Xiu *et al.*, Nat. Nanotechnol. **6**, 216 (2011).
[15] O. V. Yazyev, J. E. Moore, and S. G. Louie, Phys. Rev. Lett. **105**, 266806 (2010).
[16] P. Wei, F. Katmis, B. A. Assaf, H. Steinberg, P. Jarillo-Herrero, D. Heiman, and J. S. Moodera, Phys. Rev. Lett. **110**, 186807 (2013).
[17] P. Larson and W. R. L. Lambrecht, Phys. Rev. B **78**, 195207 (2008).
[18] M. G. Vergniory *et al.*, Phys. Rev. B **89**, 165202 (2014).
[19] S. Y. Xu *et al.*, Nat. Phys. **8**, 616 (2012).
[20] Y. L. Chen *et al.*, Science **329**, 659 (2010).
[21] Y. S. Hor *et al.*, Phys. Rev. B **81**, 195203 (2010).
[22] C. Z. Chang *et al.*, Phys. Rev. Lett. **112**, 056801 (2014).
[23] C. Z. Chang *et al.*, Adv. Mater. **25**, 1065 (2013).
[24] H. Ohno, D. Chiba, F. Matsukura, T. Omiya, E. Abe, T. Dietl, Y. Ohno, and K. Ohtani, Nature (London) **408**, 944 (2000).
[25] T. Dietl, Nat. Mater. **9**, 965 (2010).
[26] K. He, Y. Wang, and Q. K. Xue, Natl. Sci. Rev. **1**, 38 (2013).
[27] J. W. Liu, T. H. Hsieh, P. Wei, W. H. Duan, J. Moodera, and L. Fu, Nat. Mater. **13**, 178 (2014).
[28] R. M. White, *Quantum Theory of Magnetism: Magnetic Properties of Materials*, 3rd ed. Springer Series in Solid-State Sciences (Springer, Berlin; New York, 2007).
[29] J. H. Van Vleck, Rev. Mod. Phys. **25**, 220 (1953).
[30] J. J. Rehr, J. J. Kas, F. D. Vila, M. P. Prange, and K. Jorissen, Phys. Chem. Chem. Phys. **12**, 5503 (2010).
[31] K. Jorissen, J. J. Rehr, and J. Verbeeck, Phys. Rev. B **81**, 155108 (2010).
[32] J. J. Rehr, J. J. Kas, M. P. Prange, A. P. Sorini, Y. Takimoto, and F. Vila, C.R. Phys. **10**, 548 (2009).
[33] R. F. Egerton, *Electron Energy-Loss Spectroscopy in the Electron Microscope*, 2nd ed. The Language of Science (Plenum Press, New York, 1996).
[34] M. S. Dresselhaus, G. Dresselhaus, and A. Jorio, *Group Theory: Application to the Physics of Condensed Matter* (Springer-Verlag, Berlin, 2008).
[35] J. S. Dyck, P. Hajek, P. Losit'ak, and C. Uher, Phys. Rev. B **65**, 115212 (2002).